Materials Sciences and Applications, 2012, 3, 24-29
http://dx.doi.org/10.4236/msa.2012.31004 Published Online January 2012 (http://www.SciRP.org/journal/msa)

EXAFS Studies of Ruthenium Based Double Perovskite $ALaMnRuO_6$ (A = Ca, Sr, Ba)

Rubina Shaheen, Javaid Bashir, Muhammad Nasir Khan*

Physics Division, PINSTECH, Islamabad, Pakistan.
Email: *nasir@pinstech.org.pk

Received August 25th, 2011; revised November 19th, 2011; accepted December 9th, 2011

ABSTRACT

Room and liquid nitrogen temperatures Mn K-edge extended X-ray fine structure (EXAFS) studies were carried out on powder samples of $ALaMnRuO_6$ (A = Ca, Sr, Ba) perovskites. The EXAFS analysis of Mn K-edge spectra showed MnO_6 octahedra are distorted. Among the three perovskites, the polyhedral distortion is highest for $SrLaMnRuO_6$ ($\Delta = 1.4 \times 10^{-3}$). For $CaLaMnRuO_6$ ($\Delta = 0.5 \times 10^{-3}$) and $BaLaMnRuO_6$, ($\Delta = 0.7 \times 10^{-3}$), the smaller values of distortion parameters indicate that the MnO_6 octahedra are relatively regular and undistorted in the latter two systems. In $SrLaMnRuO_6$, MnO_6 distortion appears to be of orthorhombic (Q_2) type whereas for $CaLaMnRuO_6$ and $BaLaMnRuO_6$, the distortion is of tetragonal or Q_3 type. The Mn-O distances as determined from the EXAFS measurements, increases with the increase in the size of the divalent cation. No structural changes occurred in the local environment around Mn atom when the temperature was lowered from room to liquid nitrogen temperature.

Keywords: Oxides; Ceramics; EXAFS; Crystal Structure

1. Introduction

The ideal perovskite structure with stoicheometry AMO_3, where A is typically a large, low oxidation state cation, M is a smaller transition metal or lanthanide cation, has cubic symmetry with space group $Pm\bar{3}m$ [1]. The capacity of perovskite structure to incorporate almost all the elements in the periodic table except for noble gas elements, beryllium and phosphorus has resulted in materials exhibiting range of properties including dielectric, piezoelectric, ferroelectric, optical, superconducting and magnetoresistive properties [2]. The perovskite structure is viable to wide variations in compositions from the ideal formula AMO_3. These variations can be achieved by isomorphous substitutions at A or M sites, and cationic and anionic deficiencies. These can be represented as $A_{1-x}A'_xMO_3$, $AM_{1-x}M'_xO_3$. The physical properties of perovskites are shown to depend on the doping levels at the A or M sites [3-6]. For 50% substitution, such mixed system are classified as double perovskites with the formula $AA'MM'O_6$ or $A_2MM'O_6$ as reported by Anderson *et al.* (1993) in reference [7]. The lattice distortion and local structure plays an important role in the magnetoelectric transport properties of perovskite manganites, in particular its effect on the colossal magnetoresistive (CMR) properties [8-10].

Ruthenates perovskites has attracted immense interest of the physicist and chemist over the past few years [11-15]. This surge of interest in ruthenates is because of their rich variety of magnetic states exhibited by these materials. For example, $SrRuO_3$ is a 4d ferromagnetic metal [14] while $CaRuO_3$ is metallic but not magnetic; the double perovskite Sr_2YRuO_6 is an antiferromagnetic insulator; and the layered perovskite Sr_2RuO_4 is superconducting [15]. The magnetic properties of double perovskite ruthenate oxides depends on the nature of MM′ distribution over the octahedral sites [16-18].

Though the crystal structures of $ALaMnRuO_6$ (A = Ca, Sr, Ba) are well established [19-24]. However, no information is available about the local structure around the manganese in these materials. In our earlier publications, we have reported crystal structure as well as the oxidation state of Mn in $SrLaMnRuO_6$, $BaLaMnRuO_6$ and $CaLaMnRuO_6$ [21-23]. Room temperature local strucutre around Mn in $SrLaMnRuO_6$ has also been reported [21]. In the present paper, we now report the local structure around Mn in $CaLaMnRuO_6$ (CLMRO), and $BaLaMnRuO_6$ (BLMRO) at room and liquid nitrogen temperatures. In addition we also report the loal structure in $SrLaMnRuO_6$ (SLMRO) at liquid nitrogen temperature.

2. Experimental

The single-phase powder samples of $ALaMnRuO_6$ (A=

*Corresponding author.

Ca, Sr, Ba) were synthesized by conventional solid-state reaction method as reported earlier in [21]. X-ray diffraction revealed that all the samples have orthorhombic symmetry (space group Pbnm), with the tilting scheme $a^-a^-b^+$ which results in the unit cell dimension of $\sqrt{a} \times \sqrt{a} \times 2a$ (where a is the pseudocubic unit cell parameter).

Room and liquid nitrogen temperatur Mn K-edge X-ray absorption spectroscopy experiments, which include both XANES and EXAFS techniques, were performed at the XAFS beam line at ELETTRA Synchrotron Radiation Source, Trieste, Italy. Well-dispersed powder samples in cyclohexane were deposited on porous membranes. The amount of the sample was pre-calculated to obtain optimum absorption jump ($\Delta\mu \approx 1$). X-ray beam energies were tuned using a double crystal, focusing Si (111) monochromator crystals. The incident (I_o) and transmitted (I_t) beam intensities were recorded using ionization chambers filled with appropriate gases. Data were collected in three regions: 1) the pre-edge region with a step size of 5 eV to allow pre-edge background calculation and subtraction; 2) the XANES region from 30 eV below the edge to 50 eV above the absorption edge with a step size of 0.3 eV; and 3) the EXAFS region upto 7050 eV. All the edges were recorded at least twice. Raw data were corrected and converted to k-space, summed and background subtracted to yied the EXAFS function $\chi(k)$ using the EXCALIB and EXBACK Programs [25]. The edge profiles were separated from the EXAFS data and, after subtraction of the linear pre-edge background, normalized to the edge step. The data were weighted by k^3, where k is the photoelectron wavevector, to enlarge the oscillations at high k. The data were fitted using the non-linear square minimisation program EXCURV92 [26] which calculates the theoretical function using the fast curved wave theory [27]. Phase shifts corrections were calculated using Xalpha exchange and ground potentials.

3. Results and Discussion

Figure 1(a)-(b) represents the modulus of Fourier Transform (FT) extracted from the XAS data at 300 K and 80 K by measuring Mn K-edge EXAFS spectra for the three systems. The k^3-weighted $\chi(k)$ data were Fourier transformed (FT) in the k range of 2.5 - 12 $Å^{-1}$ using a Guassian window. Well defined peaks corresponding to the different coordination shells around the Mn absorbing atom are visible upto about 5 Å. The main intense peak at about 1.9 Å in the FT is associated with the MnO_6 octahedron. Further peaks around 3 - 4 Å in the FT are attributed to Mn-A/La and Mn-O-Mn interactions [8,28].

The first peak of FT, corresponding to the Mn-O, octahedra are identical for all the materials except for a slight upward shift that indicates gradual increase of the Mn-O distances with increasing size of A atom. However, there are marked differences corresponding to Mn-A/La and Mn-O-Mn interactions as we move from $CaLaMnRuO_6$ to $BaLaMnRuO_6$. The shape of these peaks are found to be dependent either on the crystallographic symmetry or the different scattering power of the divalent cations. Since, laboratory X-ray diffraction studies have revealed that all of these materials have the same orthorhombic symmetry (space group Pbnm) [21-23], these differences can only be attributed to the different scattering powers of A cations. For all three samples, nearly constant amplitudes of Mn-O peaks at 300 K and 80 K indicates that no structural changes occur in the local environment around the Mn as the temperature is lowered.

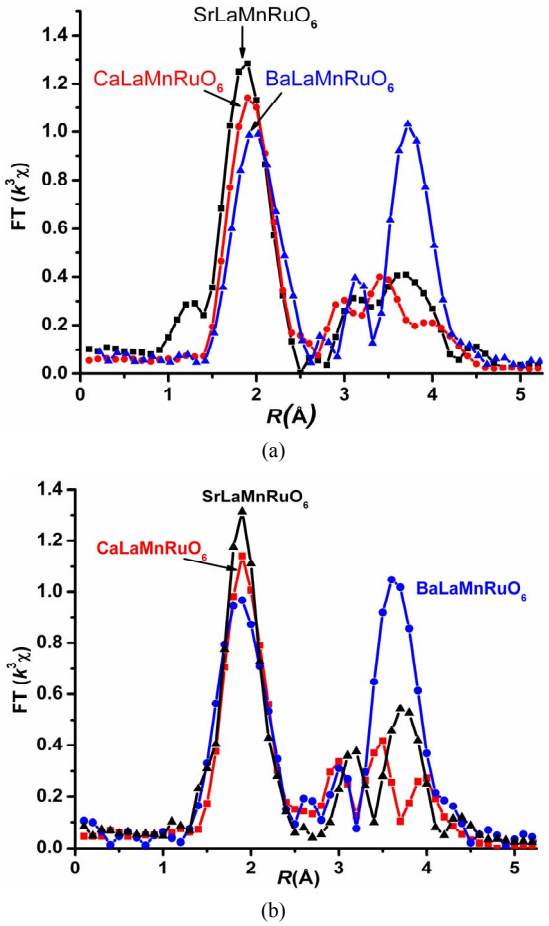

Figure 1. EXAFS fitting results (a) at room temperature and (b) liquid nitrogen temperature; experimental points (dots) and best fit (—) for comparison of three systems.

Previous neutron diffraction [19,20] and synchrotron X-ray diffraction studies [21,23] have shown that the structure of $ALaMnRuO_6$ is orthorhombic with distorted Mn/RuO_6 octahedra (**Figure 2**). Owing to the Jahn Teller effects, caused by the 3d Jahn Teller ion Mn^{3+}, distortion

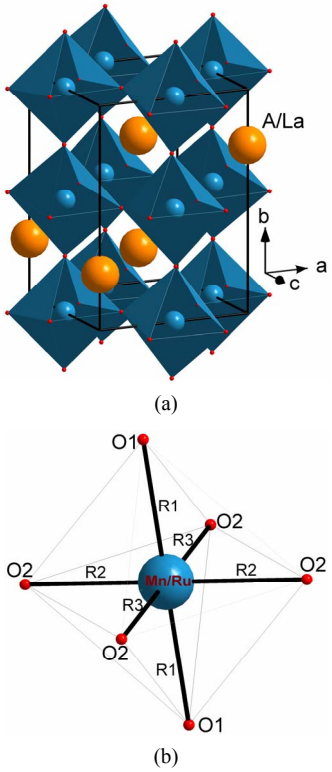

Figure 2. (a) Schematic representation of the orthorhombic *Pbnm* crystal structure of ALaMnRuO$_6$ in which A/La (A = Ca, Sr, Ba) atoms; (b) Ru/MnO$_6$ octahedron.

of MnO$_6$ produces three Mn-O bonds with equal bond distances, long (*l*), medium (*m*) and short (*s*) bonds [29, 30]. In case of CLMRO and BLMRO, the MnO$_6$ octahedra are quite regular and the spread in the bond lengths is small [22,23] whereas in SLMRO the bondlengths in the basal plane are further split into two Mn-O bonds of equal bond lengths and the structure is considerably distorted [21].

Extended X-ray absorption fine structure (EXAFS) spectroscopy provides structural information about a sample by way of the analysis of its X-ray absorption spectrum. In order to extract structural information from experimental spectra, a simple analytical expression that relates the EXAFS signal to the structural parameters is required. An EXAFS analytical expression like the one suggested by Teo [31] is:

$$\chi(k) = \sum_j \frac{N_j f_j(k) e^{-2k^2\sigma_j^2} \sin\left[2kR_j + \delta_j(k)\right]}{kR_j^2}$$

where k is the electron wave vector, N_j is the number of atoms in the j-th coordination shell, $\delta_j(k)$ is the phase shift, $f_j(k)$ is the scattering amplitude, σ_j is the Debye Waller factor in terms of a Gaussian broadening resulting from thermal and static disorder and R_j is the M-O bond length in the Mn-O octahedral (**Figure 2(b)**). Various structural parameters can be extracted by an approximate Fourier analysis of the normalized EXAFS term $\chi(k)$ [32].

In all of these perovskites oxides, the Mn ions are surrounded by six oxygen atoms forming an octahedron (**Figure 2(b)**). In cubic, undistorted perovskite structure, all the Mn-O bond distance are equal, *i.e.*, $R_1 = R_2 = R_3$. As both La and A cations are distorted from the central position in the simple cubic unit cell, making their near-neighbor oxygen environment complicated. In addition to these distortions, presence of JT distortion is also present. The six otherwise equal, Mn-O bond lengths in the tilted octahedral consequently split into pairs of unequal bond length. Distortion caused by the Jahn-Teller effect in perovskites usually involves four of the octahedral bonds (bonds involving planar oxygen, R_2 and R_3) contracting and two of the octahedral bonds (apical oxygen) lengthening which gives an elongated octahedral shape.

Different models were employed for fitting the experimental EXAFS data. In the first model (2 + 2 + 2 model), we have used three subshells each with a coordination number $N_{\text{Mn-O}} = 2$ with unequal Mn-O bondlengths. Subsequently we employed models with two sub shells, one corresponding to a Mn-O coordination number $N_{\text{Mn-O}} = 4$ at shorter distance and the other corresponding to $N_{\text{Mn-O}} = 2$ at longer distance (4 + 2 model); a model with bimodal distribution of Mn-O bonds with three longer Mn-O bonds and three shorter Mn-O bonds (3 + 3 model) and a model with one Mn-O sub shell with $N_{\text{Mn-O}} = 6$. Owing to strong correlation between coordination number (N) and Debye-Waller factor (σ^2), only the distance (R) and σ^2 were refined. Since electronic properties mainly depend on the nearest neighbours, we are focusing only on the first shell analysis.

For SLMRO, as reported previously [21] the best fit to EXAFS data were obtained for 2 + 2 + 2 model. In case of CLMRO and BLMRO, the best fits were obtained for 4 + 2 model, *i.e.* four short and two long bonds. The remanining models lead to relatively high values of Debye Waller Factors without any significant improvement in the fit. Typical fitted FT spectra at room temperature are shown in **Figure 1(a)**. The summary of the fitted structural parameters are listed in **Table 1**. The calculated interatomic distances are in good agreement with values obtained from the crystallographic measurements [19-23]. This suggests that the local structure as determined from EXAFS mathches the average structure as determined from neutron or Synchrotron X-ray diffraction. The main result is that the Mn-O distances increases with the increasing size of the divalent cation A in agreement with the shifts observed in the first peak of the FT. The slightly higher values of Debye-Waller factors suggests a site to site variation of the bond lengths in the MnO$_6$ octahedra [28].

Table 1. EXAFS parameters of the first oxygen coordination shell at Mn K-edge. *R* is the interatomic Mn-O distance, N being the coordination number and σ^2 is the Debye-Waller factor. The errors on radial distances are ±0.01 Å whereas on DW factors the error is ±0.001 Å^2.

Shell	$CaLaMnRuO_6$					$SrLaMnRuO_6$					$BaLaMnRuO_6$				
	N	*R*(Å)		$\sigma^2 \times 10^{-2}$ (Å^2)		*N*	*R*(Å)		$\sigma^2 \times 10^{-2}$ (Å^2)		*N*	*R*(Å)		$\sigma^2 \times 10^{-2}$ (Å^2)	
		300 K	80 K	300 K	80 K		300 K	80 K	300 K	80 K		300 K	80 K	300 K	80 K
Mn-O	4	1.92	1.90	0.6	0.4	2	1.87	1.85	0.9	1.4	4	1.97	1.95	0.1	0.1
Mn-O	2	2.01	1.99	0.9	0.8	2	1.95	1.95	0.6	0.4	2	2.08	2.07	0.3	0.2
Mn-O	-	-	-	-	-	2	2.05	2.02	1.4	1.8	-	-	-	-	-

There are two types of distortion modes associated with the JT distortion: Q_2 and Q_3 which are defined in terms of long (*l*), medium (*m*) and short (*s*) Mn-O bonds as:

$$Q_2 = 2(l-s)/\sqrt{2}$$
$$Q_3 = 2(2m-l-s)/\sqrt{6}$$

with *l*, *s* being the Mn-O distances in the *ab* plane and *m* is out of plane Mn-O bond length. Q_3 is a tetragonal whereas Q_2 is orthorhombic distortion [29]. In the tetragonal or Q_3 distortion the in-plane bonds extend and out of the plane bond shortens or vice versa implying that one bond length is larger than the other two. On the other hand, in the orthorhombic or Q_2 distortion, the two in plane bond lengths ($Mn\text{-}O_2$) split more symmetrically around the out of plane $Mn\text{-}O_1$ bond length. Examination of the bond lengths derived from the XAFS data reveals that in SLMRO, MnO_6 distortion appears to be of orthorhombic (Q_2) type whereas for CLMRO and BLMRO, the distortion is of tetragonal or Q_3 type.

The MnO_6 polyhedral distortion parameter Δ, frequently observed for e_g level degenerated systems such as Mn^{3+} ($t_{2g}^3 e_g^1$) containing perovskites is defined as

$$\Delta = \frac{1}{N}\sum_{n=1}^{N}\left\{\frac{d_n - \langle d\rangle}{\langle d\rangle}\right\}_n^2$$

where $\langle d\rangle$ is average Mn – O bond distance. The distortion parameters of $ALaMnRuO_6$ are listed in **Table 2**. Among the three perovskites, the polyhedral distortion is the highest for SLMRO. For CLMRO and BLMRO, the smaller values of distortion parameters indicate that the MnO_6 octahedra are relatively regular and undistorted. This result is consistent with the neutron diffraction measurements of Garanado *et al.* [19]. As the temperature is lowered, there is little change in the average bond distances and hence the distortion parameters.

Table 2. MnO6 Polyhedral distortion parameter (Δ) for $ALaMnRuO_6$ as determined from EXAFS parameters. R is the average Mn-O bond length.

Samples	T = 300 K		T = 80 K	
	$\langle R\rangle$ (Å)	$\Delta \times 10^{-3}$	$\langle R\rangle$ (Å)	$\Delta \times 10^{-3}$
$CaLaMnRuO_6$	1.95	0.5	1.93	0.5
$SrLaMnRuO_6$	1.96	1.4	1.94	1.3
$BaLaMnRuO_6$	2.01	0.7	1.99	0.8

4. Conclusion

We have carried out Mn-K-edge X-ray Absorption spectroscopy measurements to study valence state of Mn and local structure around it in single phase $ALaMnRuO_6$ perovskites prepared through solid state technique. The Mn-O distances as determined from the EXAFS measurements, increases with the increasing size of the divalent cation. No structural changes occur in the local envoirnment around Mn as the temperature is lowered from room to liquid nitrogen temperature.

5. Acknowledgements

Two of the authors (JB and RS) are grateful to the Abdus Salam International Center for Theoretical Physics (ASICTP) for the provision of financial support under the ICTP-ELETTRA user programme. The authors are also grateful to Dr. Luca Olivi for his skilful help in conducting the experiments at the XAFS beam line at the ELETTRA Synchrotron Radiation Source, Trieste, Italy.

REFERENCES

[1] R. H. Mitchell, "Perovskites: Modern and Ancient," Almaz Press, Thunder Bay, Canada, 2002.

[2] B. Raveau, "The Perovskite History: More than 60 Years of Research from the Discovery of Ferroelectricity to Colossal Magnetoresistance via High T_c Superconductivity," *Progress in Solid State Chemistry*, Vol. 35, No. 2-4, 2007, pp. 171-173. doi:10.1016/j.progsolidstchem.2007.04.001

[3] K. Kuepper, M. C. Falub, K. C. Prince, V. R. Galakhov, I. O. Troyanchuk, S. G. Chiuzbaian, M. Matteucci, D. Wett, R. Szargan, N. A. Ovechkina, Y. M. Mukovskii and M. Neumann, "Electronic Structure of A- and B-Site Doped Lanthanum Manganites: A Combined X-Ray Spectroscopic Study," *The Journal of Physical Chemistry B*, Vol. 109, No. 19, 2005, pp. 9354-9361. doi:10.1021/jp044447w

[4] A. J. Millis, "Lattice Effects in Magnetoresistive Manganese Perovskites," *Nature*, Vol. 392, No. 6672, 1998,

pp. 147-150. doi:10.1038/33017

[5] P. M. Woodward, T. Vogt, D. E. Cox, A. Arulraj, C. N. R. Rao, P. Karen and A. K. Cheetham, "Influence of Cation Size on the Structural Features of $Ln_{1/2}A_{1/2}MnO_3$ Perovskites at Room Temperature," *Chemistry of Materials*, Vol. 10, No. 11, 1998, pp. 3652-3665. doi:10.1021/cm980397u

[6] J. Guan, S. E. Dorris, U. Balachandran and M. Liu, "The Effects of Dopants and A: B Site Nonstoichiometry on Properties of Perovskite-Type Proton Conductors," *Journal of the Electrochemical Society*, Vol. 145, No. 5, 1998, pp. 1780-1786. doi:10.1149/1.1838557

[7] M. T. Anderson, K. B. Greenwood, G. A. Taylor and K. R. Poeppelmeier, "B-Cation Arrangements in Double Perovskites," *Progress in Solid State Chemistry*, Vol. 22, No. 3, 1993, pp. 197-233. doi:10.1016/0079-6786(93)90004-B

[8] D. M. A. Melo, F. M. M. Borges, R. C. Ambrosio, P. M. Pimentel, C. N. da Silva Jr. and M. A. F. Melo, "XAFS Characterization of $La_{1-x}Sr_xMnO_{3\pm\delta}$ Catalysts Prepared by Pechini's Method," *Chemical Physics*, Vol. 322, No. 3, 2006, pp. 477-484. doi:10.1016/j.chemphys.2005.09.008

[9] A. J. Millis, B. I. Shraiman, R. Mueller, "Dynamic Jahn-Teller Effect and Colossal Magnetoresistance in $La_{1-x}Sr_xMnO_3$," *Physical Review Letters*, Vol. 77, No. 1, 1996, pp. 175-178. doi:10.1103/PhysRevLett.77.175

[10] V. Krishnan, G. Bottaro, S. Gross, L. Armelao, E. Tondello and H. Bertagnolli, "Structural Evolution and Effects of Calcium Doping on Nanophasic $LaCoO_3$ Powders Prepared by Non-Alkoxidic Sol-Gel Technique," *Journal of Materials Chemistry*, Vol. 15, No. 20, 2005, pp. 2020-2027. doi:10.1039/b502470f

[11] E. Quarez, F. Abraham and O. Mentré, "Synthesis, Crystal Structure and Characterization of New 12H Hexagonal Perovskite-Related Oxides $Ba_6M_2Na_2X_2O_{17}$ (M=Ru, Nb, Ta, Sb; X=V, Cr, Mn, P, As)" *Journal of Solid State Chemistry*, Vol. 176, No. 1, 2003, pp. 137-150. doi:10.1016/S0022-4596(03)00379-7

[12] R. O. Bune, M. V. Lobanov, G. Popov, M. Greenblatt, C. E. Botez, P. W. Stephens, M. Croft, J. Hadermann and G. V. Tendeloo, "Crystal Structure and Properties of Ru-Stoichiometric $LaSrMnRuO_6$," *Chemistry of Materials*, Vol. 18, No. 10, 2006, pp. 2611-2617. doi:10.1021/cm052371q

[13] J.-W. G. Bos and J. P. Attfield, "Structural, Magnetic, and Transport Properties of $(La_{1+x}Sr_{1-x})CoRuO_6$ Double Perovskites," *Chemistry of Materials*, Vol. 16, No. 9, 2004, 1822-1827. doi:10.1021/cm0497733

[14] A. Callaghan, C. W. Moeller and R. Ward, "Magnetic Interactions in Ternary Ruthenium Oxides," *Inorganic Chemistry*, Vol. 5, No. 9, 1966, pp. 1572-1576. doi:10.1021/ic50043a023

[15] Y. Maeno, H. Hashimoto, K. Yoshida, S. Nishizaki, T. Fujita, J. G. Bednorz and F. Lichtenberg, "Superconductivity in a Layered Perovskite without Copper," *Nature*, Vol. 372, No. 6506, 1994, pp. 532-534. doi:10.1038/372532a0

[16] M. P. Attfield, P. D. Battle, S. K. Bollen , S. H. Kim, A. Powell and M. Workman, "Structural and Electrical Studies of Mixed Copper/Ruthenium Oxides and Related Compounds of Zinc and Antimony," *Journal of Solid State Chemistry*, Vol. 96, No. 2, 1992, pp. 344-359. doi:10.1016/S0022-4596(05)80268-3

[17] P. D. Battle, T. C. Gibbs, C. W. Jones and F. Studer, "Spin-Glass Behavior in Sr_2FeRuO_6 and $BaLaNiRuO_6$: A Comparison with Antiferromagnetic $BaLaZnRuO_6$," *Journal of Solid State Chemistry*, Vol. 78, No. 2, 1989, pp. 281-293. doi:10.1016/0022-4596(89)90109-6

[18] P. D. Battle, C. W. Jones and F. Studer, "The Crystal and Magnetic Structures of Ca_2NdRuO_6, Ca_2HoRuO_6, and Sr_2ErRuO_6," *Journal of Solid State Chemistry*, Vol. 90, No. 2, 1991, pp. 302-312. doi:10.1016/0022-4596(91)90147-A

[19] E. Granado, Q. Huang, J. W. Lynn, J. Gopalakrishnan and K. Ramesha, "Crystal Structures and Magnetic Order of $La_{0.5+d}A_{0.5-d}Mn_{0.5+e}Ru_{0.5-e}O_3$ (A = Ca, Sr, Ba): Possible Orbital Glass Ferromagnetic State," *Physical Review B*, Vol. 70, No. 21, 2004, pp. 214416.1-214416.7.

[20] R. I. Das, J.-Q. Yan and J. B. Goodenough, "Ruthenium Double Perovskites: Transport and Magnetic Properties," *Physical Review B*, Vol. 69, No. 9, 2004, pp. 094416.1-094416.16.

[21] J. Bashir, R. Shaheen and M. N. Khan, "Structural Characterization of $SrLaMnRuO_6$ by Synchrotron X-Ray Powder Diffraction and X-Ray Absorption Spectroscopy," *Solid State Sciences*, Vol. 10, No. 5, 2008, pp. 638-644. doi:10.1016/j.solidstatesciences.2007.10.011

[22] K. Shahzad, R. Shaheen, M. Nasir Khan and J. Bashir, "Crystal Structure and Valence State of Mn in $BaLaMnRuO_6$," *Journal of Physics D*: *Applied Physics*, Vol. 41, No. 17, 2008, p. 175413. doi:10.1088/0022-3727/41/17/175413

[23] M. N. Khan , R. Shaheen and J. Bashir, "Neutron, Synchrotron X-Ray Diffraction and X-Ray Absorption Studies of $CaLaFeMnO_6$ Double Perovskite," *Solid State Sciences*, Vol. 10, No. 11, 2008, pp. 1634-1639. doi:10.1016/j.solidstatesciences.2008.02.007

[24] S. S. Pillai, S. N. Jammalamadaka and P. N. Santhosh, "Magnetotransport Properties of Ba_2MnRuO_6 and $LaBaMnRuO_6$," *Magnetics, IEEE Transactions*, Vol. 43, No. 6, 2007, pp. 3076-3078. doi:10.1109/TMAG.2007.892568

[25] N. Binstead, J. W. Campbell, S. J. Gurman and P. C. Stephenson, "SERC Daresbury Laboratory EXCALIB and EXBACK Programs," 1990.

[26] N. Binstead, J. W. Campbell, S. J. Gurman and P. C. Stephenson, "SERC Daresbury Laboratory EXCURV92 Programme," 1991.

[27] S. J. Gurman, N. Binsted and I. Ross, "A Rapid, Exact-Curved-Wave Theory for EXAFS Calculations," *Journal of Physics C*: *Solid State Physics*, Vol. 17, No. 1, 1984, p. 143.

[28] T. Shibata, B. A. Bunker and J. F. Mitchell, "Local Distortion of MnO_6 Clusters in the Metallic Phase of $La_{1-x}Sr_xMnO_3$," *Physical Review B*, Vol. 68, No. 2, 2003, pp. 024103.1-024103.10.

[29] J. Kanamori, "Super Exchange Interaction and Symmetry Properties of Electron Orbitals," *Journal of Physics and*

Chemistry of Solids, Vol. 10, No. 2-3, 1959, pp. 87-98. doi:10.1016/0022-3697(59)90061-7

[30] G. Matsumoto, "Study of $(La_{1-x}Ca_x)MnO_3$. I. Magnetic Structure of $LaMnO_3$," *Journal of the Physical Society of Japan*, Vol. 29, No. 3, 1970, pp. 606-615. doi:10.1143/JPSJ.29.606

[31] B. K. Teo, "EXAFS: Basic Principles and Data Analysis," Springer Verlag, New York, 1986.

[32] D. E. Sayers, E. A. Stern and F. W. Lytle, "New Technique for Investigating Noncrystalline Structures: Fourier Analysis of the Extended X-Ray—Absorption Fine Structure," *Physical Review Letters*, Vol. 27, No. 18, 1971, pp. 1204-1207. doi:10.1103/PhysRevLett.27.1204

